Self-assembling of tetradecylammonium chain on swelling high charge micas (Na-Mica-3 and Na-Mica-2): Effect of alkylammonium concentration and mica layer charge

M. Carolina Pazos,[1] Agustín Cota,[2] Francisco J. Osuna, [3] Esperanza Pavón,[3,4] María D. Alba[,3]*

[1] *Escuela de Ciencias Químicas, Universidad Pedagógica y Tecnológica de Colombia UPTC. Avda. Central del Norte, Vía Paipa,Tunja, Boyacá, Colombia.*

[2] *Laboratorio de Rayos-X. Centro de Investigación, Tecnología e Innovación de la Universidad de Sevilla (CITIUS), Universidad de Sevilla. Avda. Reina Mercedes, 4, 41012 Sevilla, Spain.*

[3] *Instituto Ciencia de los Materiales de Sevilla (ICMS), Consejo Superior de Investigaciones Científicas-Universidad de Sevilla, Avda. Américo Vespucio, 49, 41092 Sevilla, Spain.*

[4] *Centers for the Development of Nanoscience and Nanotechnology, CEDENNA, 9170124 Santiago, Chile.*

KEYWORDS. Organomica, hydrophobicity, alkylammonium, cation exchange capacity, swelling high-charged micas.

ABSTRACT. A family of tetradecylammonium micas is synthesized using synthetic swelling micas with high layer charge ($Na_nSi_{8-n}Al_nMg_6F_4O_{20}\cdot XH_2O$, where n= 2 and 3) exchanged with tetradecylammonium cations. The molecular arrangement of the surfactant is elucidated on the basis of XRD patterns and DTA. The ordering conformation of the surfactant molecules into the interlayer space of micas is investigated by IR/FT, ^{13}C, ^{27}Al and ^{29}Si MAS NMR. The structural arrangement of the tetradecylammonium cation in the interlayer space of high-charge micas is more sensitive to the effect of the mica layer charge at high concentration. The surfactant arrangement is found to follow the bilayer-paraffin model for all values of layer charge and surfactant concentration. However, at initial concentration below the mica CEC a lateral monolayer is also observed. The amount of ordered conformation *all-trans* is directly proportional of the layer charge and surfactant concentration.

INTRODUCTION

The term organoclays (OC) denotes a family of hydrophobic materials, obtained by modifying clays and clay minerals with various organic compounds through intercalation processes and surface grafting.[1,2,3,4,5] Organoclays have important practical applications, notably as adsorbents of organic pollutants[6,7,8,9] and as components in the formation of clay polymer nanocomposites[2,10,11,12]. A large volume of literature has been accumulated over the past two decades on various aspects of OC research, including i) synthesis and characterization[4,13,14]; ii) surface properties and stability[4,13,14]; iii) production of clay-based nanocomposites[10,11,12,15]; and iv) synthesis of novel materials using the OC as precursors[16,17].

A more recent development that has attracted much interest is the organo-functionalization of a new family of swelling high-charged micas.[18,19,20] Those synthetic micas have a charge density similar to brittle micas but with a higher swelling capacity, higher crystallinity and controllable composition.[21,22,23] In this way, those synthetic micas overcome some limitations of the natural clay minerals to be used as host materials.

Dodecylammonium and octadecylammonium have been successfully intercalated in the interlayer space of a whole family of synthetic high-charge mica. In all case, a paraffin-type bilayer structure was observed with a tilt angle between 51º and 65º.[19,20] However, the structural arrange of alkylammonium in the interlayer space for the lowest chain length (12 *vs* 18 carbon atoms) was more sensitive to the mica charge because the adsorbed amount of alkylammonium was slightly less than the cation exchange capacity of mica. In the case of the highest chain length (18 *vs* 12 carbon atoms), alkylammonium was adsorbed by: exchange reaction and on the surface by hydrophobic interaction.[20]

Many studies have been performed to analyze the effect of alkyl chain length,[24,25,26,27] the species of cationic surfactant[28,29], and its-concentration[30,31,32] on the d-spacing and the alkyl chain arrangements on organoclays. Among them, the most important factor was found to be the surfactant concentration. Lagaly[33] reported that the surfactant package on clay minerals changes from a lateral monolayer to a lateral bilayer, and, finally to a pseudotrimolecular layer or a paraffin-type monolayer depending on the nature of surfactant and layered silicate. Later on, also the d-spacing was found to increase with the increment on the surfactant concentration, allowing the alkyl chains to adopt a paraffin-type bilayer with a tilting angle of 35° at a surfactant concentration higher than its exchange capacity (CEC).[34] Moreover, this alkyl chain arrangement but with a larger tilting angle (60°) has also been reported in $KNiAsO_4$.[35] However, the effect of surfactant concentration on the hydrophobicity, d-spacing and alkyl chain arrangement of modified swelling high-charged micas has not been analyzed yet.

Thus, the aim of this work is to evaluate the arrangement and interlayer properties of different swelling high charge micas, Na-Mica-n (n is the layer charge; n=2 and 3), as a function of alkylammonium concentration and mica layer charge. Based on our previous work,[20] tetradecylammonium has been chosen, it has an carbon chain length between the 12 and 18 as previously analyzed, to satisfy the 0.5-10 CEC of the micas.

EXPERIMENTAL DETAILS

a. Materials. Na-Mica-n (n=2 and 3) were synthesized using the NaCl-melt method following a similar procedure to that described by Alba et al.[23] Their structural formulae are $Na_n[Si_{8-n}Al_n]Mg_6O_{20}F_4 \cdot zH_2O$, where *n* represent the charge per unit cell (n=2 and 3) and *z* is the number of water molecules. The starting materials employed were SiO_2 (Sigma; CAS no. 112945-52-5,

99.8% purity), $Al(OH)_3$ (Riedel-de Haën; CAS no. 21645-51-2, 99% purity), MgF_2 (Aldrich; CAS no. 20831-0, 98% purity), and NaCl (Panreac; CAS no. 131659, 99.5% purity). Stoichiometric proportions of reactants were weighed and mixed in an agate mortar. The molar ratio between the reactants were $(8-n)SiO_2$:$(n/2)Al_2O_3$:$6MgF_2$:$(2n)$NaCl. It was added twice the amount of NaCl to ensure the complete charge balance with Na^+ cation into the interlayer space.[36] The optimal amount of mixture reaction for grinding was up to 2 g per batch during 30 min for ensuring the homogeneity of the mixture in an agate mortar. The heat treatments were carried out in a closed Pt crucibles at 900 ºC during 15 h using a heating rate of 10 ºC·min^{-1}. The product was washed with distilled water and the solid was separated by filtration, dried at room temperature and then ground in the agate mortar.

b. Preparation of tetradecylammonium micas. The organomicas were prepared by a cation-exchange reaction between the micas and variable concentration of tetradecylammonium salt to satisfy the 0.5, 1, 2, 3 or 10 times the cation exchange capacity (CEC) of Na-Mica-n. Thus, the primary amine was dissolved in an equivalent amount of HCl (0.1 M) and the resulting mixture stirred for 3 h at 80 °C. The tetradecylammonium dispersion was then mixed with 0.6 g of Na-Mica-n and stirred for 3 h at 80 °C. After adding hot deionized water, the mixture was stirred for 30 min at 50 °C and then the dispersion was centrifuged at 10,000 r.p.m. for 20 minutes. The product was dissolved in a hot ethanol-water mixture (1:1) and stirred for 1 h at 50 ºC and then centrifuged.[13] The precipitate was dried at room temperature. The sample will be named as C_{14}-Mica-n-m; where *n* is the interlayer charge 2 or 3 and *m* is the initial concentration of the tetradecylammonium salt (m=0, 0.5, 1, 2, 3 and 10 CEC). The samples C_{14}-Mica-n-0 corresponds to the as-synthesized sample Na-Mica-n.

c. Techniques. Simultaneous TG/DTA measurements were performed at the Departamento de Cristalografía, Mineralogía y Química Agrícola (University of Seville, Spain) using a NETZSCH (STA 409 PC/PG) instrument which is equipped with a Pt/Pt-Rh thermocouple for direct measurement of the temperature at the sample/reference crucible from room temperature up to 900 °C (heating rate: 10 °C·min^{-1}) in an atmosphere of N_2. Approximately 150 mg of sample was used and the DTA reference was pure aluminum oxide.

X-ray diffraction (XRD) patterns were obtained at the CITIUS X-ray laboratory (University of Seville, Spain) on a Bruker D8 Advance instrument equipped with a Cu K_α radiation source operating at 40 kV and 40 mA. Diffractograms were obtained in the 2θ range of 1–70° with a step size of 0.05° and a step time of 3.0 s.

FTIR spectra were recorded in the range 4000–300 cm^{-1} by the Spectroscopy Service of the ICMS (CSIC-US, Seville, Spain), as KBr pellets, using a Nicolet spectrometer (model 510P) with a nominal resolution of 4 cm^{-1}.

Single-pulse (SP) MAS-NMR experiments were recorded on the samples where the tetradecylammonium concentration were the lowest and the highest because they should exhibit appreciable differences at short-range order, C_{14}-Mica-n-m (n=2 and 3; m=0.5 and 10 CEC), the C_{14}-Mica-n-2 was also measured for comparison with previous works[19,20]. The measurements were carried out on the Spectroscopy Service of the ICMS (CSIC-US, Seville, Spain) using a Bruker DRX400 spectrometer equipped with a multinuclear probe. Powdered samples were packed into 4-mm zirconia rotors and spun at 10 kHz. ^{27}Al MAS NMR spectra were acquired at a frequency of 104.26 MHz, using a pulse width of 0.92 μs (π/2 pulse length = 9.2 μs) and a delay time of 0.1 s. ^{23}Na MAS NMR spectra were recorded at 105.84 MHz with pulse widths of 2.0 μs (π/2 pulse length=12.0 μs) and a delay time of 0.1 s. ^{29}Si MAS NMR spectra were

acquired at a frequency of 79.49 MHz, using a pulse width of 2.7 μs (π/2 pulse length = 7.1 μs) and a delay time of 3 s. ^{13}C MAS NMR spectra were recorded at 104.26 MHz with proton decoupling, a pulse width of 2.5 μs (π/2 pulse length = 7.5 μs) and a delay time of 2 s. The chemical shift values are reported in ppm with respect to 0.1 M $AlCl_3$ solution for ^{27}Al, 0.5 M NaCl solution for ^{23}Na and tetramethylsilane for ^{29}Si and ^{13}C.

RESULTS AND DISCUSSIONS

a. Adsorption in the interlayer space of organomicas: Hydrophobicity and stability. To investigate the structure and properties of the tetradecylammonium molecules adsorbed onto Na-Mica-n, the adsorbed amount of the organic cations are monitored by TG.[37,38,39] Table 1 shows the content of water and surfactant obtained from the analysis of the TG curves, where the amount of interlayer water is determined from the weight loss in the temperature range of 25–170 °C and the amount of the adsorbed tetradecylammonium molecules is determined from the weight loss between 170 and 900 °C.[40]

The amount of adsorbed tetradecylammonium is higher in C_{14}-Mica-3 than in C_{14}-Mica-2, thus, the main adsorption may occur by cation exchange, and this adsorption is proportional to the initial concentration of alkylammonium. In C_{14}-Mica-n-m ($m<2$), tetradecylammonium is adsorbed in less amount than their CEC (ca. 0.60 CEC for m=0.5 and ca. 0.95 CEC for m=1). At $m\geq2$ the alkylammonium cations adsorption exceeds the mica exchange capacity and this excess is stabilized by van der Waals interactions between alkyl chains.[41,42,43,44] This excess is only slightly higher than the CEC for C_{14}-Mica-3-m, for m=2 and 3, but is five time higher than CEC for m=10. The alkylammonium concentration necessary to satisfy the layer charge is higher for

143 C_{14}-Mica-3 and, thus, the packing density is higher and the van der Waals interactions between
144 alkyl chains are favored.

145 DTG analysis (Figure 1) suggests two distinct states for the intercalated surfactant molecules:
146 (i) the first one is associated to the thermal decomposition of intercalated alkylammonium, with
147 stronger interaction, and, thus, requires a higher temperature (442 ºC) to decompose[45,46], and, (ii)
148 the second one is due to the presence of ion-pair alkylammonium ions,[20] with weaker interaction,
149 whose decomposition temperature is slightly lower (ca. 350 ºC). For m=0.5 only the
150 decomposition at the higher temperature is observed and agrees with the adsorption of surfactant
151 of ca. 60 % of their CEC (Table 1). As the initial concentration of alkylammonium increases the
152 decomposition at lower temperature is more relevant and becoming the dominant process for
153 C_{14}-Mica-3-10.

154 Mica surface properties can be altered from hydrophilic to organophilic by the exchange of the
155 hydrated Na^+ interlayer cation by an organic one,[47] and consequently causing a drastic
156 diminishing of the water content. Thus, whereas the water content on Na-Mica-n-0 is found to be
157 between 3.17 and 3.63 molecules per unit cell; it decreases on C_{14}-Mica-n-m due to the
158 replacement of Na^+ for the organic cations favoring the hydrophobic character of the interlayer
159 space (Table 1). For $m \leq 1$, a gradual decrease of interlayer water with alkylammonium
160 concentration is observed, being in concordance with an increasing in the exchange of inorganic
161 cations by the organic ones. However, for $m \geq 2$, the amount of water slightly increases with
162 alkylammonium concentration due to that is adsorbed not only by cation exchange reaction but
163 also by ionic pair which could adsorb some water molecules in the hydrophilic head of the
164 cationic surfactant.

The hydrophilic character of the interlayer space after the adsorption of different concentrations of tetradecylammonium can be explained from the analysis of the ^{23}Na MAS NMR spectra (Figure 2). The ^{23}Na MAS NMR spectra of C_{14}-Mica-n-0 (Na-Mica-n) is characterized by two signals one at 3.7 ppm due to sodalite[48], and other at -10.1 ppm due to fully hydrated exchangeable sodium[49,50]. When the initial concentration of the alkylammonium increases the signal of interlayer sodium decreases, this effect is more evident as the layer charge increases. It corroborates the increasing hydrophopic character of the interlayer space and that the slightly increasing of water content observed for m≥2 (see Table 1) is due to water associated at ionic pair tetradecylammonium. The interlayer sodium is completely replaced in C_{14}-Mica-3-10 in good agreement with the extremely high content of adsorbed tetradecylammonium (Table 1).

b. Tetradecylammonium package on organomicas. The analysis of the *00l* reflections of the XRD patterns (Figure 3) can be shed a light on the long-range structural order of the organomicas. The basal spacing of Na-Mica-n is 1.20 nm, which corresponds to Na^+ in the interlayer space surrounded by one water pseudomonolayer.[23] The exchange reaction between Na^+ and the tetradecylammonium cation causes an increase in the basal spacing (d_{001}). An unique and well-ordered sequence of the *00l* reflections is only observed for the C_{14}-Mica-3-10, and that corresponds to a basal spacing of 4.02 nm, an interlayer gallery height of 3.08 nm (Table 2), compatible with paraffinic bilayer -type structures.[51,52,53] Paul et al.[54] observed that the surfactant molecules adopt an arrangement that allow them to pack efficiently; therefore, the maximum concentration of adsorbed tetradecylammonium in C_{14}-Mica-3-10 could favor a high and ordered packing which is reflected in a well-ordered sequence of the *00l* reflections. However, in the other C_{14}-Mica-n-m, at least two *00l* reflections sequences are observed. The splitting of the *00l*

188 reflections cannot be explained by inhomogeneity of the charge distribution, which is not
189 expected as the starting material is the same for all the micas, and in C_{14}-Mica-3-10, a unique *00l*
190 sequence is observed.

191 In C_{14}-Mica-n-0.5, the most intense *001* reflection corresponds to a basal spacing of 2.48 nm
192 (for n=2) and 3.50 nm (for n=3), which could be compatible with a paraffin conformation but a
193 small *001* reflection due to a basal spacing of 1.43 and 1.34 nm (for n=2 and 3, respectively) is
194 also observed and is compatible with a monolayer conformation (Table 2).[55] Hydrocarbon chains
195 lying flatly on the surface would make the clay hydrophobic even at low surface coverage and it
196 can explain the decreases in the interlayer space water content although only the 60 % of CEC
197 was satisfied in C_{14}-Mica-2-0.5.

198 The arrangement of a lateral monolayer of the alkyl chains evolves to a paraffin-type bilayer in
199 the interlayer of micas with the increase in surfactant concentration.[33] The reason is that the
200 interlayer alkylammonium molecules cannot form parallel layer arrangements in the interlayer
201 space of the mica when the interlayer cation density is higher than 1.94.[20]

202 The d-spacing of the main *001* reflection increases with the increase surfactant concentration
203 and the layer charge, as previously reported in montmorillonites. **¡Error! Marcador no definido.**,[56] Mainly,
204 the alkyl chains take the arrangement of a paraffin-type bilayer with a tilting angle ranging
205 between 24º and 59º (Table 2).

206 IR/FT spectroscopy is used to support the evidence of compaction of the surface film on the
207 clay minerals. The IR/FT absorption bands at 1450–1480 cm^{-1} (Figure 4) can be ascribed to the
208 methylene scissoring mode. They have been found to be sensitive to the interchain interactions
209 and consequently, can be used as a probe of the packing arrangements in alkyl chain
210 assemblies.[57,58] When the methylene groups are found in an all parallel arrangement, a triclinic

211 subcell, a sharp and narrow singlet at 1472 cm^{-1} is observed.[58] However, when they are displayed
212 in a hexagonal phase, the band position moves up to 1468 cm^{-1} and when they conform an
213 orthorhombic subcell, the bands change to a doublet at 1462 and 1473 cm^{-1}.[58] With the exception
214 of C_{14}-Mica-3-10, in all the samples (Figure 4) the band is a singlet located at 1468 ± 1 cm^{-1},
215 reflecting that the surfactant surface is arranged in a hexagonal phase.[59] For C_{14}-Mica-3-10,
216 where the interlayer Na^+ is completely replaced by tetradecylammonium, a doublet at 1462 and
217 1475 cm^{-1} is observed indicating an orthorhombic cell with intermolecular interaction between
218 the two adjacent hydrocarbon chains.[57] Those interactions are favored by the high adsorption of
219 tetradecylammonium, ca. 500 % of its CEC (Table 1).

220 The CH_2 stretching bands are generally the strongest bands and the frequency of these υ_{as} and
221 υ_s bands are sensitive to the *gauche*/*trans* conformer ratio of the hydrocarbon chains. A shift
222 from low frequencies characteristic of highly ordered, all-*trans* conformations, to higher
223 frequencies and increased width is accompanied as the number of *gauche* conformers (the
224 "disorder" of the chain) increases.[59] Independently of the initial tetradecylammonium
225 concentration, those bands are centered at 2919 ± 1 cm^{-1} and 2849 ± 1 cm^{-1}, for υ_{as} and υ_s
226 vibrational modes respectively, (Figure S1) which denotes a high proportion of *all-trans*
227 arrangement.[60]

228 Substantial information of the tetradecylammonium structure can be obtained from the ^{13}C
229 MAS NMR analysis (Figure S2). In general, the spectra are similar to those previously reported
230 for C_x-Mica-n (n=2, 3 or 4; and x=12 or 18).[19,20] As previously reported,[19,20] the spectra show a
231 set of narrowed signals (marked with asterisk in Figure S2) that is likely corresponds to
232 tetradecylammonium with a different package in good agreement with the various *001*
233 reflections families observed by XRD. It is also remarkable a narrow and intense peak at ca. 15

ppm from the terminal peak in C_{14}-Mica-3-10 where tetradecylammonium was adsorbed in an amount over the 500 % of CEC. Among the signals, the resonances at 30-33 ppm, internal methylene (Figure 5), are important to be analyzed since information on the chain configuration can be obtained.[61] That signal is the convolution of two peaks at ca. 30 ppm (mixed *gauche* and *trans,* disordered configuration) and at ca. 33 ppm (all-*trans*, ordered configuration).[62,63] When the interlayer tetradecylammonium concentration increases, the proportion of disordered configuration diminishes as the alkyl chain freedom decreases. These data are consistent with results reported in the literature, where He et al.[64] observed that the all-*trans* conformer is favored at high amine concentration. The high proportion of C_{14}-Mica-3-0.5 in disordered configuration may be explained by its high available volume per tetradecylammonium cations (0.66 nm^3/mol in C_{14}-Mica-3-0.5 compared to 0.10 nm^3/mol in C_{14}-Mica-3-10).

c. Analysis of organomicas framework. The short-range framework structural order of the organomicas is analyzed by ^{29}Si and ^{27}Al MAS NMR.

The ^{29}Si MAS NMR spectra (Figure 6) is characterized by a set of bands in the range between δ = –70 to –95 ppm, consistent with the existence of four $Q^3(q\text{Al})$ ($0 \leq q \leq 3$) environments.[65] While the spectra of C_{14}-Mica-n-0 is consistent with those previously reported for these micas,[19] the $Q^3(3\text{Al})$ signals of C_{14}-Mica-n-m (m≥0.5) are shifted up to ca. 2.1 and 2.5 ppm, for n= 2 and 3 respectively, towards lower frequencies. A similar shift has already been observed in the ^{29}Si frequencies of high charge swelling silicates, and was attributed to the formation of inner sphere complexes between the interlayer cations and the basal oxygen of the silicate tetrahedral layer.[66] In the same manner, and according to the high tilt angle observed by XRD (Table 2), the ^{29}Si signal shifts in C_{14}-Mica-n is caused by the inclusion of the NH_3^+ into the pseudohexagonal hole of the silicate framework. The above results reinforce the proposed bi-layer structure with alkyl

chains in an all-*trans* configuration, and that the polar part of the surfactant is close to the basal oxygen plane.

All the ^{29}Si MAS NMR spectra of C_{14}-Mica-n-m (m≥0.5) show similar relative peak intensities in comparison with C_{14}-Mica-n-0. The ^{27}Al MAS NMR spectra of C_{14}-Mica-n-0 (Figure S3) are characterized by a signal at ca. 60 ppm typical of tetrahedral aluminum. Not additional signals due to a different Al coordination number after tetradecylammonium adsorption is observed. Therefore, the exchange process does not alter the Si and Al distribution.

CONCLUSIONS

Tetradecylammonium has been intercalated in the interlayer space of synthetic swelling high-charge micas. Both the interlayer charge of mica and the initial concentration of tetradecylammonium determine the adsorbed amount and, therefore, the arrangement of the organic cations in the interlayer space.

The effect of the mica layer charge is more evident at high concentration. The molecular arrangement of the surfactant is found to follow the bilayer-paraffin model for all values of layer charge and surfactant concentration. However, at initial concentration below the mica CEC, a lateral monolayer is also observed.

The alkyl chain of the tetradecylammonium adopts a configuration that is a mixture between ordered (all-*trans*) and disordered (mixed *gauche-trans*); the amount of the disordered arrangement being higher in C_{14}-Mica-n-0.5 where the CEC of the mica is not satisfied.

For a high adsorbed tetradecylammonium, C_{14}-Mica-3-10, a unique family of *00l* plane and a change from hexagonal phase to orthorhombic cell is observed.

Corresponding Author

*E-mail: alba@icmse.csic.es

Author Contributions

The manuscript was written through contributions of all authors. All authors have given approval to the final version of the manuscript.

ACKNOWLEDGMENT

We would like to thank the Junta de Andalucía (Spain) and FEDER (Proyecto de Excelencia de la Junta de Andalucía, project P12-FQM-567) for providing financial support. We also thank to ENRESA and CIEMAT for providing samples and by their support. Dr. Pavón also thanks Andalucía Talent Hub program, given by Agencia Andaluza del Conocimiento and co-financed by the 7th Framework Programme, Marie Curie Actions: People, Co-funding of Regional, National, and International Programmes and by Consejería de Economía, Innovación, Ciencia y Empleo, Junta de Andalucía.

REFERENCES

(1) Bergaya, F.; Lagaly, G. Surface modification of clay minerals. *Appl. Clay Sci.* **2011**, *19*, 1–3.

(2) Bergaya, F.; Jaber, M.; Lambert, J-F. *Organophilic Clay Minerals, Chapter 2.* In: Galimberti,M. (Ed.), Rubber-Clay Nanocomposites: Science, Technology and Applications. John Willey & Sons, 2011; pp. 45–86.

(3) He, H.P.; Tao, Q.; Zhu, J.X.; Yuan, P.; Shen, W.; Yang, S.Q. Silylation of clay mineral surfaces. *Appl. Clay Sci.* **2013**, *71*, 15–20.

(4) Lagaly, G.; Ogawa, M.; Dékany, I. *Clay Minerals Organic Interactions*. Chapter 10.3, Handbook of Clay Science, In: Bergaya, F., Lagaly, G. (Eds.), 2nd edition. Developments in Clay Science, vol. 5A. Elsevier, 2013; pp. 435–505.

(5) Paiva, L.; Morales, A.; Valenzueladiaz, F. Organoclays: properties, preparation and applications. *Appl. Clay Sci.* **2008**, *42*, 8–24.

(6) Bergaya, F.; Lagaly, G. *General Introduction: Clays, Clay Minerals and Clay Science Chapter 1,* Handbook of Clay Science, In: Bergaya, F., Lagaly, G. (Eds.), 2nd edition. Developments in Clay Science, vol. 5A. Elsevier, 2013; pp. 1–19.

(7) Stockmeyer, M.R. Adsorption of organic compounds on organophilic bentonites. *Appl. Clay Sci.* **1991**, *6*, 39–57.

(8) Theng, B.K.G.; Churchman, G.J.; Gates, W.P.; Yuan, G. *Organically Modified Clays for Pollutant Uptake and Environmental Protection.* In: Huang, Q., Huang, P.M., Violante, A. (Eds.), Soil Mineral-Microbe-Organic Interactions: Theories and Applications. Springer-Verlag, Berlin, 2008; pp. 145–174.

(9) Zhu, L.Z.; Chen, B.L.; Shen, X.Y. Sorption of phenol, p-nitrophenol, and aniline to dual-cation organobentonites from water. *Environ. Sci. Technol*. **2000**, *34*, 468–475.

(10) Bergaya, F.; Detellier, C.; Lambert, J-F.; Lagaly, G. Introduction on Clay Polymer Nanocomposites (CPN), Chapter 13, Handbook of Clay Science, In: Bergaya, F., Lagaly, G. (Eds.), 2nd edition. Developments in Clay Science, vol. 5A. Elsevier, 2013; pp. 655–677.

(11) Ray, S.S.; Okamoto, M. Polymer/layered silicate nanocomposites: a review from preparation to processing. *Prog. Polym. Sci.* **2003**, *28*, 1539–1641.

(12) Theng, B.K.G. *Formation and Properties of Clay-Polymer Complexes*, 2nd edition. Elsevier, Amsterdam, 2012.

(13) Lagaly, G. Characterization of clays by organic compounds. *Clay Miner.* **1981**, *16*, 1–21.

(14) Zhu, J.X.; He, H.P.; Guo, J.G.; Yang, D.; Xie, X.D. Arrangement models of alkylammonium cations in the interlayer of HDTMA+ pillared montmorillonites. *Chin. Sci. Bull.* **2003**, *48*, 368–372.

(15) Lambert, J.F.; Bergaya, F. *Smectites-Polymer Nanocomposites*, Chapter 13.1, Handbook of Clay Science, In: Bergaya, F., Lagaly, G. (Eds.), 2nd edition. Developments in Clay Science, vol. 5A. Elsevier, 2013; pp. 699–706.

(16) Bergaya, F.; Lagaly, G. *Intercalation Processes of Layered Minerals, in Layered Mineral Structures and Their Application in Advanced Technology*. Chapter 6 In: Brigatti, M.F., Mottana, A. (Eds.), EMU notes in Mineralogy, 2011, vol. 11, pp. 259–284.

(17) Ishii, R.; Nakatsuji, M.; Ooi, K. Preparation of highly porous silica nanocomposites from clay mineral: a new approach using pillaring method combined with selective leaching. *Micro. Meso. Mater.* **2005**, *79*, 111–119.

(18) Franklin, K.R.; Lee, E. Synthesis and ion-exchange properties of Na-4-mica. *J. Mater. Chem.* **1996**, *6*, 109-115.

(19) Alba, M.D.; Castro, M.A.; Orta, M.M.; Pavón, E.; Pazos, M.C.; Valencia, J.S. Formation of Organo-Highly Charged Mica. *Langmuir* **2011**, *27*, 9711-9718.

(20) Pazos, M.C.; Castro, M.A.; Orta, M.M.; Pavón, E.; Valencia, J.S.; Alba, M.D. Synthetic High-Charged Organomica: Effect of the Layer Charge and Alkyl Chain Length on the Structure of the Adsorbed Surfactants. *Langmuir* **2012**, *28*, 7325-7332.

(21) Kodama, T.; Komarneni, S. Na-4-mica: Cd^{2+}, Ni^{2+}, Co^{2+}, Mn^{2+} and Zn^{2+} ion exchange. *J. Mater. Chem.* **1999**, *9*, 533-539.

(22) Park, M.; Lee, D.H.; Choi, C.I.; Kim, S.S.; Kim, K.S.; Choi, J. Pure Na-4-mica: Synthesis and Characterization. *Chem. Mater.* **2002**, *14*, 2582-2589.

(23) Alba, M. D.; Castro, M. A.; Naranjo, M.; Pavón, E. Hydrothermal Reactivity of Na-n-Micas (n = 2, 3, 4) *Chem. Mater.* **2006**, *18*, 2867-2872.

(24) Yilmaz, N.; Yapar, S. Adsorption properties of tetradecyl- and hexadecyl trimethylammonium bentonites. *Appl. Clay Sci.* **2004**, *27*, 223–228.

(25) Calderon, J.U.; Lennox, B.; Kamal, M.R. Thermally stable phosphonium-montmorillonite organoclays. *Appl. Clay Sci.* **2008**, *40*, 90–98.

(26) Chen, H.; Zhou, L.M.; Jiang, X.H.; Lu, F.; Zhou, Y.F.; Yin, W.M.; Ji, X.Y. Modification of montmorillonite surfaces using a novel class of cationic gemini surfactants. *J. Coll. Inter. Sci.* **2009**, *332*, 16–21.

(27) Frost, R.L.; Xi, Y.F.; He, H.P. Modification of the surfaces of Wyoming montmorillonite by the cationic surfactants alkyl trimethyl, dialkyl dimethyl, and trialkylmethyl ammonium bromides. *J. Coll. Inter. Sci.* **2007,** *305*, 150–158.

(28) Duchet-Rumeau, J.; Livi, S.; Pham, T.N.; Gerard, J.F. A comparative study on different ionic liquids used as surfactants: Effect on thermal and mechanical properties of high-density polyethylene nanocomposites. *J. Coll. Inter. Sci.* **2010**, *349*, 424–433.

(29) Tiwari, R.R.; Khilar, K.C.; Natarajan, U. Synthesis and characterization of novel organo-montmorillonites. *Appl. Clay Sci.* **2008**, *38*, 203–208.

(30) Lagaly, G. Inorganic layer compounds. *Die Naturwissenschaften* **1981**, *68*, 82–88.

(31) Wen, X.; He, H.; Zhu, J.; Jun, Y.; Ye, C.; Deng, F. Arrangement, conformation, and mobility of surfactant molecules intercalated in montmorillonite prepared at different pillaring

reagent concentrations as studied by solid-state NMR spectroscopy. *J. Coll. Inter. Sci.* **2006**, *299*, 754–760.

(32) Xi, Y.F.; Frost, R.L.; He, H.P.; Kloprogge, T.; Bostrom, T. Modification of Wyoming montmorillonite surfaces using a cationic surfactant. *Langmuir* **2005**, *21*, 8675–8680.

(33) Lagaly, G. Interaction of alkylamines with different types of layered compounds. *Sol. State Ionics* **1986**, *22*, 43–51

(34) Yui, T.; Yoshida, H.; Tachibana, H.; Tryk, D.A.; Inoue, H. Intercalation of polyfluorinated surfactants into clay minerals and the characterization of the hybrid compounds. *Langmuir* **2002**, *18*, 891–896.

(35) Beneke, K.; Lagaly, G. The Brittle Mica-Like $KNiAsO_4$ and its Organic Derivatives. *Clay Miner.* **1982**, *17*, 175–183.

(36) Esfandiari, A.; Nazokdast, H.; Rashidi, A. S.; Yazdanshenas, M. E. Review of polymer-organoclay nanocomposites. J. Appl. Sci. 2008, 8, 545-561.

(37) Osman, M. A.; Seyfang, G.; Suter, U. W. Two-Dimensional Melting of Alkane Monolayers Ionically Bonded to Mica. *J. Phys. Chem. B* **2000**, *104,* 4433-4439.

(38) Osman, M. A.; Suter, U. W. Surface Treatment of Calcite with Fatty Acids: Structure and Properties of the Organic Monolayer. *Chem. Mater*. **2002**, 14, 4408-4415.

(39) Osman, M. A.; Ploetze, M.; Suter, U. W. Surface treatment of clay minerals — thermal stability, basal-plane spacing and surface coverage. *J. Mater. Chem.* **2003**, *13*, 2359-2366.

(40) Xie, W.; Gao, Z.; Pan, W. P.; Hunter, D.; Singh, A.; Vaia, R. Thermal Degradation Chemistry of Alkyl Quaternary Ammonium Montmorillonite. *Chem. Mater.* **2001**, *13*, 2979-2990.

(41) Narine, D. A.; Guy, R. D. Interactions of some large organic cations with bentonite in dilute aqueous systems. *Clays Clay Miner.* **1981**, *29*, 205-212.

(42) Rosen, M. J. *Surfactants and Interfacial Phenomena;* ed. John Wiley & Sons, New York, 1999

(43) Tahani, A.; Karroua, M.; van Damme, H.; Levitz, P.; Bergaya, F. Adsorption of a Cationic Surfactant on Na-Montmorillonite: Inspection of Adsorption Layer by X-Ray and Fluorescence Spectroscopies. *J. Colloid Interface Sci.* **1999**, *216*, 242-249.

(44) Ijdo, W. L.; Pinnavaia, T. J. Staging of Organic and Inorganic Gallery Cations in Layered Silicate Heterostructures. *J. Solid State Chem.* **1998**, *139*, 281-289.

(45) Onal, M. Examination of some commercial sorptive organobentonites. *Turk. J. Chem.* **2007**, *31*, 579-588.

(46) Yariv, S. The role of charcoal on DTA curves of organo-clay complexes: an overview. *Appl. Clay Sci.* **2004**, *24*, 225-236.

(47) Jaynes, W. F.; Boyd, S. A. Clay Mineral Type and Organic Compound Sorption by Hexadecyltrimethylammonium-Exchanged Clays. *Soil Sci. Soc. Am. J.* **1991**, *55*, 43-48.

(48) Johnson, G.M.; Mead, P. J.; Dann, S. E.; Weller, M. T. Multinuclear MAS NMR studies of sodalitic framework materials. *J. Phys. Chem. B* **2000**, *104*, 1454-1463.

(49) Zeng, Z.; Matuschek, D.; Studer, A.; Schwicker, C.; Pöttgen, R.; Eckert, H. Synthesis and characterization of inorganic-organic hybrid materials based on the intercalation of stable organic radicals into a fluoromica clay. *Dalton Trans.* **2013***, 42*, 8585-8596.

(50) Casal, B.; Aranda, P.; Sanz, J.; Ruiz-Hitzky, E. Interlayer adsorption of macrocyclic-compounds (crown-ethers and cryptands) in 2/1 phyllosilicates .2. Structural features. *Clay Miner*. **1994**, *29*, 191-203.

(51) Brindley, G. W. Complexes of primary amines with montmorillonite and vermiculite. *Clay Miner.* **1965**, *6*, 91-96.

(52) Johns, W. D.; Sen Gupta, P. K. Vermiculite-alkyl ammonium complexes. *Am. Mineral*. **1967**, *52*, 1706-1724.

(53) Brindley, G.W.; Hofmann R.W. Orientation and packing of aliphatic chain molecules on montmorillonite: in *Clays and Clay Minerals, Proc. 9th Natl. Conf. West Lafayette, Indiana, 1960*, Ada Swineford, ed., Pergamon Press, New York, 1962**,** 546-556.

(54) Paul, D.R.; Zeng, Q.H.; Yu, A.B.; Lu, G.Q. The interlayer swelling and molecular packing in organoclays. *J. Coll. Inter. Sci.* **2005**, *292*, 462-468.

(55) Lagaly, G.; Weiss, A. Arrangement and orientation of cationic tensides on silicate surfaces. 3. Paraffin-like structures in alkylammonium layer-silicates with an average layer load (vermiculite). *Kolloid Z. Z. Polym*. **1970**, *238*, 485-&.

(56) Fornes, T.D.; Yoon, P.J.; Hunter, D.L.; Keskkula, H.; Paul, D.R. Effect of organoclay structure on nylon 6 nanocomposite morphology and properties. *Polymer* **2002**, *43*, 5915-5933.

(57) Casal, H.L.; Mantsch, H.H.; Cameron, D.G.; Snyder, R.G. Interchain vibrational coupling in phase-II(hexagonal) n-alkanes *J. Chem. Phys.* **1982**, *7*, 2825-2830.

(58) Venkataraman, N.V.; Vasudevan, S. Conformation of methylene chains in an intercalated surfactant bilayer. *J. Phys. Chem. B* **2001**, *105*, 1805-1812.

(59) Weers, J.G.; Scheuing, D.R. Fourier Transform Infrared Spectroscopy in Colloidal and Interface Science, in: D.R. Scheuing (Ed.), ACS Symposium Series 447, American Chemical Society,Washington, DC, 1990; p. 87.

(60) Li, Z.; Jiang, W.T.; Hong, H. An FTIR investigation of hexadecyltrimethylammonium intercalation into rectorite. *Spectrochim. Acat A.* **2008**, *71*, 1525-1534.

(61) Wang, L.Q.; Liu, J.; Exarhos, G.J.; Flanigan, K.Y.; Bordia, R. Conformation Heterogeneity and Mobility of Surfactant Molecules in Intercalated Clay Minerals Studied by Solid-State NMR. *J. Phys. Chem. B*. **2000**, *104*, 2810-2816.

(62) Vaia, R. A.; Teukolsky, R. K.; Giannelis, E. P. Interlayer Structure and Molecular Environment of Alkylammonium Layered Silicates. *Chem. Mater.* **1994**, *6*, 1017-1022.

(63) Yu, X.; Zhao, L.; Gao, X.; Zhang, X.; Wu, N. The intercalation of cetyltrimethylammonium cations into muscovite by a two-step process: II. The intercalation of cetyltrimethylammonium cations into Li-muscovite. *J. Solid State Chem.* **2006**, *179*, 1525-1535.

(64) He, H.; Frost, R. L.; Deng, F.; Zhu, J.; Wen, X.; Yuan, P. Conformation of Surfactant Molecules in the Interlayer of Montmorillonite Studied by ^{13}C MAS NMR. *Clays Clay Miner.* **2004**, *52*, 350-356.

(65) Engelhardt, G.; Michel, D. *High Resolution Solid State NMR of Silicates and Zeolites*. Ed. Wiley, New York. 1987.

(66) Pavón, E.; Castro M.A.; Naranjo, M.; Orta, M.M.; Pazos, M.C.; Alba, M.D. Hydration properties of the synthetic high-charge micas saturated with different cations: An experimental approach. *Amer. Miner.* **2013**, *98*, 394-400.

Table 1. Water and tetradecylammonium contents of the C_{14}-Mica-n-m (n=2 and 3)

n	m	25º-170º C		170º-900º C		
		%	mol H_2O/ mol mica[b]	%[a]	mol C_{14}/ mol mica[b]	%CEC
2	0	6.6	3.17	0.9	-	--
	0.5	2.2	1.30	24.7	1.20	60.0
	1	0.1	0.07	34.7	1.90	95.0
	2	0.3	0.21	39.4	2.30	114.8
	3	0.4	0.28	40.2	2.36	118.2
	10	0.3	0.23	44.9	2.83	141.6
3	0	7.3	3.63	1.2	-	--
	0.5	3.5	2.40	34.1	1.90	63.4
	1	0.0	0.00	44.3	2.84	94.7
	2	0.3	0.26	51.2	3.65	121.7
	3	0.3	0.25	50.7	3.59	119.5
	10	0.7	1.46	87.1	15.18	506.1

[a] % weight loss of the dry samples

[b] It has been calculated taking into account the unit cell formulae $(C_{14})_mNa_{n-m}(Si_{8-n}Al_n)Mg_6O_{20}F_4$; n=2 or 3

Table 2. Geometrical and Package Parameters of the C_{14}-Mica-n-m (n=2 and 3)

	C_{14}-Mica-2					C_{14}-Mica-3				
m	0.5	1	2	3	10	0.5	1	2	3	10
d_{001}	3.51^{i}	4.08^{i}	4.19^{i}	4.06^{i}	4.18^{i*}	3.50^{i*}	4.05^{i*}	4.18^{i*}	4.05^{i*}	4.02
(nm)	2.48^{ii*}	2.65^{ii*}	3.06^{ii*}	3.14^{ii*}	3.63^{ii*}	2.56^{ii}	2.99^{ii}	3.06^{ii}	3.49^{ii}	
	1.43^{iii}				3.13^{iii}	1.34^{iii}	2.66^{iii}		3.01^{iii}	
					2.40^{iv}					
h[a]	2.57	3.14	3.25	3.12	3.24^{*}	2.56^{*}	3.11^{*}	3.24^{*}	3.11^{*}	3.08
(nm)	1.54^{*}	1.71^{*}	2.12^{*}	2.20^{*}	2.69^{*}	1.62	2.05	2.12	2.55	
	0.49				2.19	0.40	1.72		2.07	
					1.46					
V[b]	1.27	1.55	1.61	1.54	1.60^{*}	1.26^{*}	1.54^{*}	1.60^{*}	1.54^{*}	1.52
(nm^3)	0.76^{*}	0.84*	1.05^{*}	1.09^{*}	1.33^{*}	0.80	1.01	1.05	1.26	
	0.24				1.08	0.20	0.85		1.02	
					0.72					
α[c]	42.70	55.94	59.04	55.41	58.75^{*}	42.49^{*}	55.14^{*}	58.75^{*}	55.14^{*}	54.36
(º)	23.97^{*}	26.82^{*}	34.01^{*}	35.48^{*}	45.22^{*}	25.31	32.74	34.01	42.29	
	--				35.30	--	26.99		33.10	
					22.66					

[i-iv] from the [*00l*]$^{i-iv}$ planes of Figure 3

* from the most intense *00l* reflection

[a] $h=d_{001}-0.94$ and it is the high of interlayer gallery

[b] $V=h\cdot a\cdot b$ (a=0.534 nm, b=0.925 nm) and it is the interlayer volume

[c] $h=2\cdot[(n_c-1)\cdot 0.126+0.131]\cdot \sin\alpha$; where α is the tilt angle of the alkylchain and n_c is the number of carbon atoms in the alkyl chain (n_c=14)

FIGURE CAPTIONS

Figure 1. DTG curves of the C_{14}-Mica-n-m (n=2 or 3 and m=0.5, 1, 2, 3 and 10 CEC) in the tetradecylammonium decomposition temperature range.

Figure 2. ^{23}Na MAS NMR spectra of the C_{14}-Mica-n-m (n=2 or 3 and m=0, 0.5, 1, 2, 3 and 10 CEC).

Figure 3. XRD patterns of the C_{14}-Mica-n-m (n=2 or 3 and m=0, 0.5, 1, 2, 3 and 10 CEC).

Figure 4. The methylene scissoring vibrational region of the IR/FT spectra of the C_{14}-Mica-n-m (n=2 or 3 and m=0.5, 1, 2, 3 and 10 CEC).

Figure 5. Internal methylene groups region of the ^{13}C MAS NMR raw spectra (left) and deconvoluted spectra (right) of the C_{14}-Mica-n-m (n=2 or 3 and m=0.5, 2 and 10 CEC). The light grey area corresponds to the *trans* configuration contribution (I_t) and the dashed light grey area corresponds to the *trans-gauche* configuration contribution (I_{t-g}).

Figure 6. ^{29}Si MAS NMR spectra of the C_{14}-Mica-n-m (n=2 or 3 and m=0, 0.5, 2 and 10 CEC). Dashed line indicates the $Q^3(q\text{Al})$ environments.

Figure 1

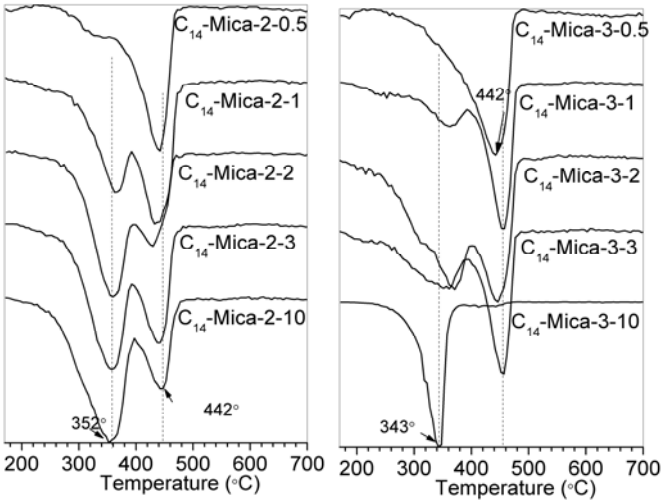
C14-Mica-2-0.5
C14-Mica-2-1
C14-Mica-2-2
C14-Mica-2-3
C14-Mica-2-10
352°
442°
200 300 400 500 600 700
Temperature (°C)
C14-Mica-3-0.5
442°
C14-Mica-3-1
C14-Mica-3-2
C14-Mica-3-3
C14-Mica-3-10
343°
200 300 400 500 600 700
Temperature (°C)

Figure 2

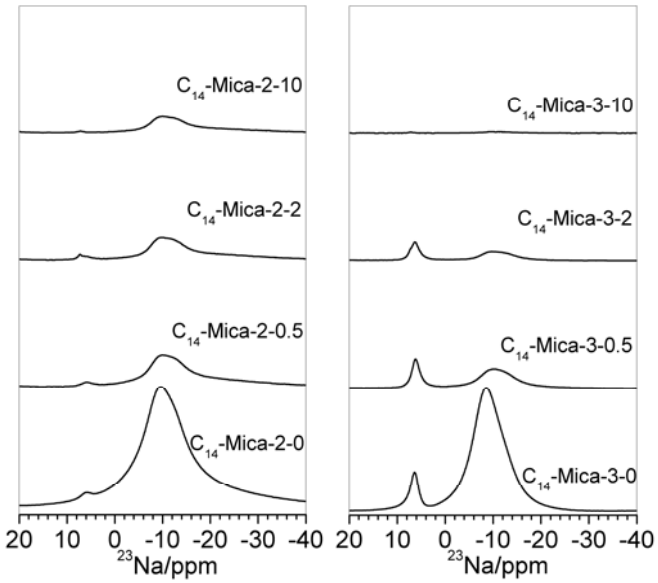
C14-Mica-2-10
C14-Mica-2-2
C14-Mica-2-0.5
C14-Mica-2-0
C14-Mica-3-10
C14-Mica-3-2
C14-Mica-3-0.5
C14-Mica-3-0
20 10 0 -10 -20 -30 -40
23Na/ppm
20 10 0 -10 -20 -30 -40
23Na/ppm

Figure 3

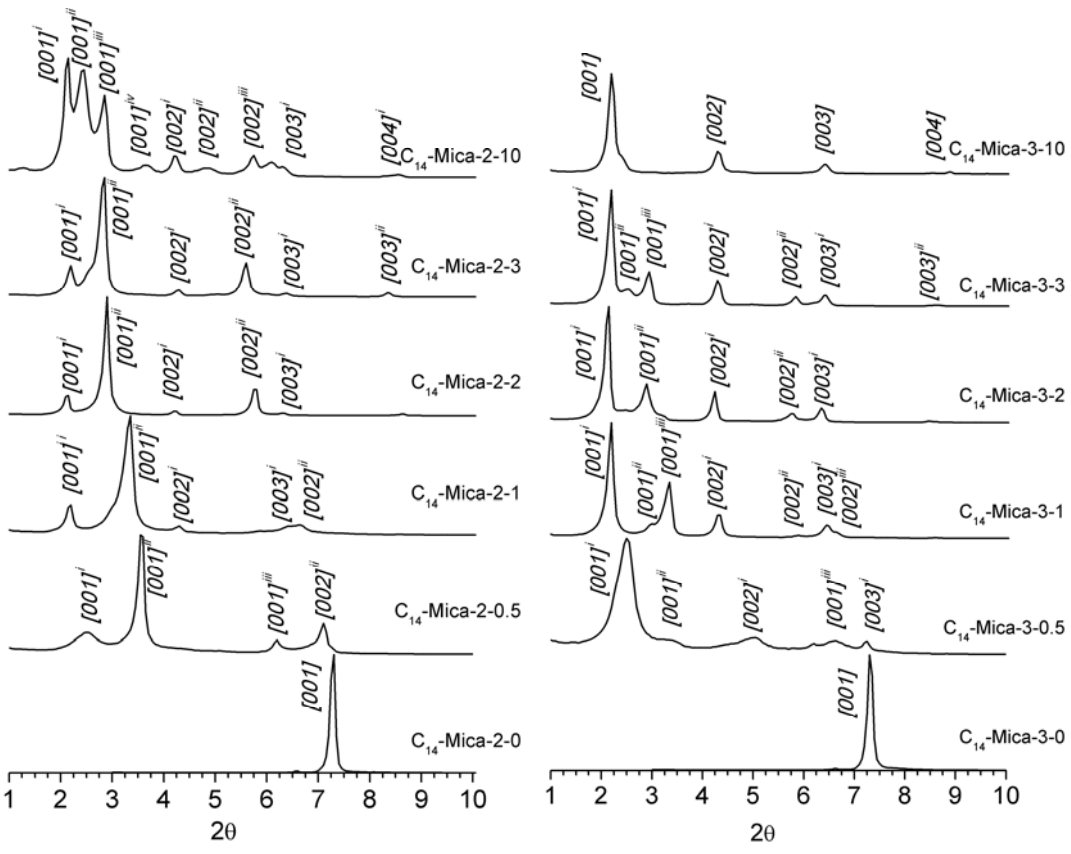
[001]
[002]
[003]
[004]
C14-Mica-2-10
C14-Mica-2-3
C14-Mica-2-2
C14-Mica-2-1
C14-Mica-2-0.5
C14-Mica-2-0
C14-Mica-3-10
C14-Mica-3-3
C14-Mica-3-2
C14-Mica-3-1
C14-Mica-3-0.5
C14-Mica-3-0
1 2 3 4 5 6 7 8 9 10
2θ

Figure 4

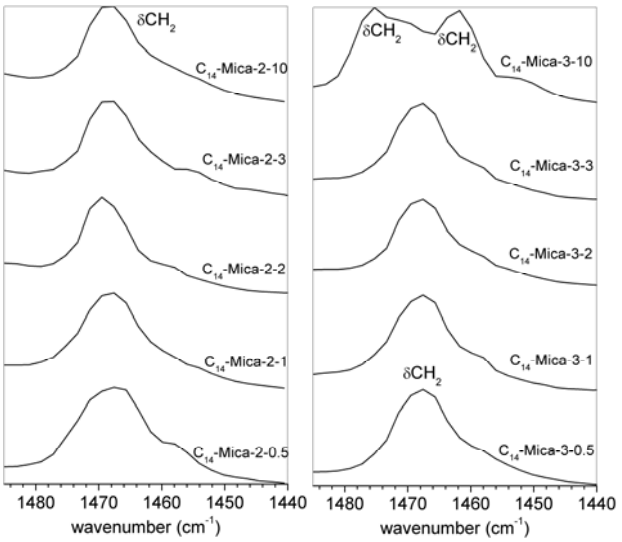
δCH2
C14-Mica-2-10
C14-Mica-2-3
C14-Mica-2-2
C14-Mica-2-1
C14-Mica-2-0.5
1480 1470 1460 1450 1440
wavenumber (cm-1)
δCH2
δCH2
C14-Mica-3-10
C14-Mica-3-3
C14-Mica-3-2
C14-Mica-3-1
δCH2
C14-Mica-3-0.5
1480 1470 1460 1450 1440
wavenumber (cm-1)

Figure 5

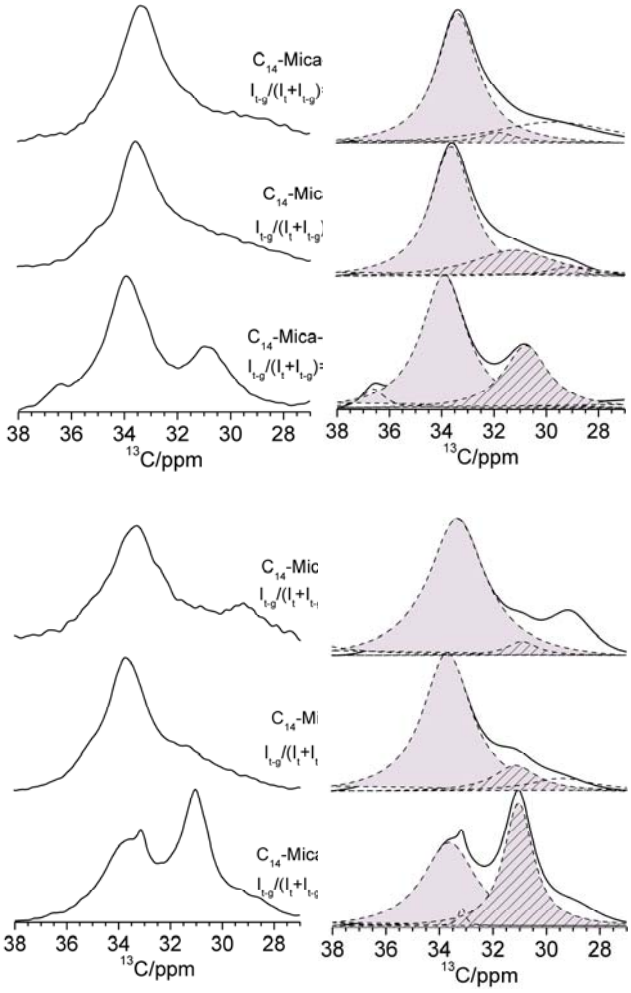
C14-Mica
C14-Mic
C14-Mica-
38 36 34 32 30 28
13C/ppm
38 36 34 32 30 28
13C/ppm
C14-Mic
C14-Mi
C14-Mica
38 36 34 32 30 28
13C/ppm
38 36 34 32 30 28
13C/ppm

Figure 6

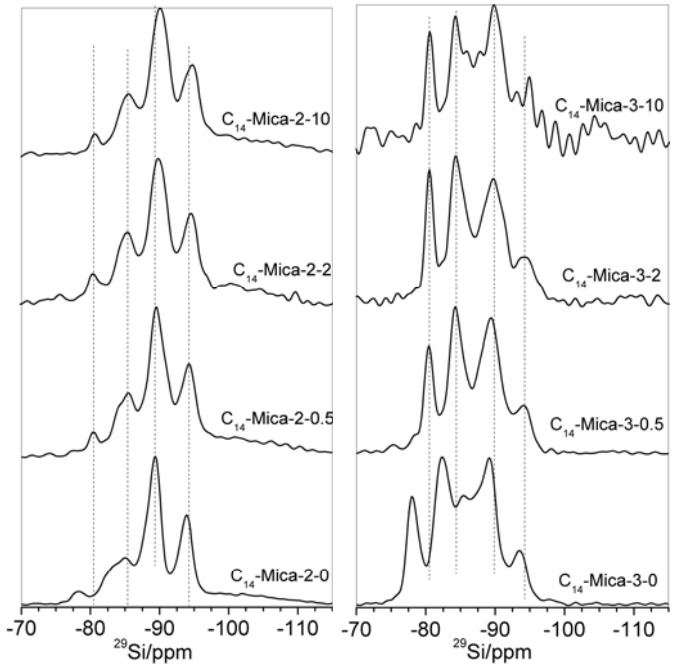
C14-Mica-2-10
C14-Mica-2-2
C14-Mica-2-0.5
C14-Mica-2-0
C14-Mica-3-10
C14-Mica-3-2
C14-Mica-3-0.5
C14-Mica-3-0
-70
-80
-90
-100
-110
29Si/ppm